

Article

Thermodynamic Assessment of the Fe–Mn–Ni System and Diffusion Mobility of Its Face-Centered Cubic Phase

Min Wang ^{1,2} , Guodong Fan ³, Chengyang Ma ⁴, Yu Mei ⁴, Tao Luo ⁴, Weisen Zheng ^{4,*} and Jiang Wang ⁵ ¹ School of Mechatronic Engineering and Automation, Shanghai University, Shanghai 200444, China² Engineering Research Center of Unmanned Intelligent Marine Equipment, Ministry of Education, 99 Shangda Rd., Shanghai 200444, China³ Luoyang Ship Material Research Institute, Xiamen 361100, China⁴ State Key Laboratory of Advanced Special Steel & Shanghai Key Laboratory of Advanced Ferrometallurgy & School of Materials Science and Engineering, Shanghai University, Shanghai 200444, China⁵ Guangxi Key Laboratory of Information Materials, Guilin University of Electronic Technology, Guilin 541004, China

* Correspondence: wszheng@shu.edu.cn

Abstract: Through extrapolation of updated binary descriptions, the Fe–Mn–Ni system was thermodynamically elucidated in a self-consistent way. The obtained thermodynamic description was confirmed to be reliable by measuring phase equilibria at relatively low temperatures. Our current thermodynamic evaluation can describe the phase stabilities over a wide temperature range and provide a reliable thermodynamic factor for the diffusion mobility optimization. For the face-centered cubic (FCC) phase in the investigated alloy system, optimization of diffusion mobilities was accomplished with the CALPHAD method. Interdiffusivities were extracted based on the composition-distance profiles of diffusion couples investigated herein. Through comprehensive diffusion behavior comparisons, our proposed diffusion mobilities were confirmed.

Keywords: thermodynamic assessment; diffusion mobility; FCC; Fe–Mn–Ni; CALPHAD



Citation: Wang, M.; Fan, G.; Ma, C.; Mei, Y.; Luo, T.; Zheng, W.; Wang, J. Thermodynamic Assessment of the Fe–Mn–Ni System and Diffusion Mobility of Its Face-Centered Cubic Phase. *Processes* **2023**, *11*, 3216. <https://doi.org/10.3390/pr11113216>

Academic Editors: Blaž Likozar and Jacopo Donnini

Received: 11 October 2023

Revised: 18 October 2023

Accepted: 25 October 2023

Published: 13 November 2023



Copyright: © 2023 by the authors. Licensee MDPI, Basel, Switzerland. This article is an open access article distributed under the terms and conditions of the Creative Commons Attribution (CC BY) license (<https://creativecommons.org/licenses/by/4.0/>).

1. Introduction

Growing attention has been received by medium-Mn steels owing to their excellent mechanical properties. Such outstanding properties are attributed to the retained austenite. The retained austenite has the transformation-induced plasticity effect during deformation. The effect can enhance work-hardening and also release local stress concentration, leading to high tensile strength and elongation. In fact, the retained austenite is usually obtained through the intercritical annealing between the start and finish temperatures of the transformation from ferrite or martensite to austenite. Thus, knowledge of the phase stabilities and diffusion behavior is crucial to determine the intercritical annealing temperature and time. Generally, the phase transformation from the ferrite or martensite to austenite during the intercritical annealing can be simulated using the moving boundary model in the DICTRA software [1]. The simulation is based on the thermodynamic and mobility databases, which can be established with the CALPHAD (CALculated PHase Diagram) method. Taking thermodynamics as an example, the greatest advantage of this method is that it can consider all available experimental data on phase diagram, thermochemical properties, and ab initio data to ensure the reliability of thermodynamic models. Moreover, the thermodynamic functions can be related to the entire composition and temperature ranges through the CALPHAD method. Note that the CALPHAD-type optimization is usually used for binary and ternary systems rather than higher order systems, because higher order interaction parameters are negligibly weak. Hence, to obtain thermodynamic and diffusion mobility descriptions of medium-Mn steels, reliable descriptions of their ternary sub-systems are required first.

Fe–Mn–Ni, as an important ternary, was thermodynamically evaluated by Zhang et al. [2], where the thermodynamic parameters of the binary Fe–Mn system by Huang [3], Fe–Ni by Servant et al. [4], and Mn–Ni by Liu [5] were used. The thermodynamic description can reproduce experimental phase equilibria for ternary Fe–Mn–Ni. Recently, Wang [6] reassessed the Fe–Ni system after critically reviewing all experimental information, and both the thermochemical properties and phase diagram data were well described. This new exploration into the binary Fe–Ni requires a re-assessment of ternary Fe–Mn–Ni to keep the thermodynamic database consistent for medium-Mn steels. Additionally, as stated in the review by Zhang et al. [2], all available experimental data about Fe–Mn–Ni alloys were collected at relatively high temperatures (above 1073 K). Therefore, those experimental phase equilibria below 1073 K were investigated in the present study.

Diffusion mobilities have been critically assessed for the FCC phase in binary Fe–Mn, Fe–Ni, and Mn–Ni alloys separately by Liu et al. [7], Wang [6], and Zhu et al. [8]. Nevertheless, accurate diffusion mobilities for FCC Fe–Mn–Ni alloys are still lacking. Moreover, the diffusivities in the FCC Fe–Mn–Ni system have never been explored. Hence, our present study measured the interdiffusion coefficients and evaluated the diffusion mobilities of FCC Fe–Mn–Ni systems by using the CALPHAD approach.

All in all, the aim of the present study is to improve the thermodynamic description of the Fe–Mn–Ni system and to obtain a self-consistent description of diffusion mobilities in FCC Fe–Mn–Ni alloys.

2. Literature Review

2.1. Thermodynamics

There have been repeated evaluations of the Fe–Mn alloys in extant literature [3,9–12]. Early evaluations [3,10,11] were made after the description of pure Mn was renovated. Among them, the evaluation by Huang [3] is universally acknowledged and adopted in the majority of databases. Re-evaluation of the binary was accomplished by Witusiewicz et al. [12] with the utilization of independent experimental data concerning the mixing enthalpy of the liquid Fe–Mn system, the formation enthalpy of the FCC Fe–Mn system, as well as the heat capacities of the FCC and BCC Fe–Mn systems [13]. Particular emphasis was placed on the martensitic FCC→HCP transition on the Fe-rich side. Nonetheless, in the re-evaluation [12], the Gibbs energy appears to be quite lower for the HCP phase on the Mn-rich side than for the FCC phase. Nakano and Jacques [14] explored how the thermodynamic variables of the HCP phase impacted the stacking fault energy and subsequently reappraised this phase. Their HCP phase elucidation would result in a miscibility gap when the Mn composition was high. Djurovic et al. [15] somewhat adjusted the parameters for the HCP phase provided by Huang [3] for better consistency with the measured temperatures of the martensitic transition reported by Cotes et al. [16]. The HCP phase displays more rational Gibbs energy on the Mn-rich side compared to that in references [12] and [14]. Therefore, the modification of the HCP phase by Djurovic et al. [15] was adopted in the present study, along with the description of stable phases by Huang [3].

Several research groups [4,17–21] have evaluated the Fe–Ni system, a highly crucial binary. Lee [17] revised the liquid phase based on the first thermodynamic evaluation by Xing et al. [18]. Servant et al. [4] used the order/disorder model to describe the L1₂ phase. The disordered part is the Gibbs energy of the FCC phase, whereas the ordered part is calculated using the four-sublattice model. This thermodynamic elucidation by Servant et al. [4] was widely accepted. After their work, Cacciamani et al. [19] thermodynamically evaluated the binary assisted by *ab initio* calculations, where ordered phases were considered on the basis of FCC and BCC lattices. Nevertheless, the calculated liquidus and solidus temperatures in the Fe-rich part were inconsistent with the experimental data. Moreover, the calculated L1₂/BCC + L1₂ phase boundary deviated greatly from the experimental finding. Although Franke and Seifert [20] described the phase diagram for Fe–Ni well, the calculated activities in the FCC and liquid phases deviated from the experimental ones largely. Recently, Ohnuma et al. [21] measured the BCC–FCC phase equilibria within a

temperature scope from 673 to 1073 K and reassessed the Fe–Ni binary. However, the BCC/BCC + FCC boundary was different from prior experimental outcomes. Additionally, the calculated $L1_2$ phase region was not well reproduced. More recently, Wang [6] from our team evaluated the Fe–Ni binary after critically reviewing all experimental information and thermodynamic descriptions. Both the thermochemical properties and phase diagram data were preferably described using model parameters by Wang [6]. Thus, our current research adopted the thermodynamic description offered by Wang [6].

Liu [5] reviewed the entire experimental information along with thermodynamic elucidations about the Mn–Ni system, and then reassessed the binary. The thermodynamic description given by Liu [5] was widely accepted in most thermodynamic databases. In contrast to Liu's description [5], all early descriptions [22–24] showed more or less deviations from the experimental data. For instance, Miettinen [22] described the intermetallic compounds as line compounds, ignoring their homogeneity ranges. Guo and Du [23] did not consider the disorder/order transformation in the Mn–Ni system. Therewith, Franke [24] revised the description given by Guo and Du [23] by using the two- and four-sublattice models to describe the ordered phases. However, both descriptions by Guo and Du [23] and Franke [24] ignored the phase diagram data measured by Ding [25]. Therefore, the present study used the description by Liu [5].

In the case of the Fe–Mn–Ni ternary, the only thermodynamical evaluation was performed by Zhang et al. [2]. They measured the phase transformation temperatures and also determined the phase equilibria of seven Fe–Mn–Ni alloys before the thermodynamic assessment. They used the thermodynamic parameters provided by Huang [3] for the Fe–Mn binary, by Servant et al. [4] for Fe–Ni, and by Liu [5] for Mn–Ni, which were not same as those utilized herein. Hence, our present study reassessed the ternary system based on the updated binary descriptions.

2.2. Diffusion Mobility

Optimization of diffusion mobilities has been achieved by Bae et al. [26] and Liu et al. [7] in the case of FCC Fe–Mn alloys. Bae et al. [26] only considered experimental tracer and interdiffusion coefficient data but ignored intrinsic diffusion coefficient data. Liu et al. [7] evaluated all experimental diffusion coefficient data and then assessed the diffusion mobilities which could well reproduce the diffusion behavior of the FCC Fe–Mn system. Moreover, the mobility description was successfully applied to the Fe–Mn–C ternary. Therefore, our present study adopted the mobility parameters from Liu et al. [7].

Jönsson [27], Xia et al. [28], and Wang [6] made diffusion mobility assessments for the FCC phase in the Fe–Ni binary, respectively. Jönsson [27] made the first complete mobility evaluation based on available experimental data. Hence, the mobility description by Jönsson [27] has been applied to many multicomponent systems. However, Xia et al. [28] noticed that the Fe impurity diffusion in FCC Ni at low temperatures calculated by Jönsson [27] deviated from experimental data. Thus, Xia et al. [28] revised the mobility for the Fe impurity diffusion in FCC Ni. More lately, Wang [6] reevaluated the mobilities in FCC Fe–Ni alloys because of the thermodynamic assessment of the Fe–Ni binary. Preferable agreement was noted between the computations and the experimental diffusion coefficients. Hence, the diffusion mobilities by Wang [6] were used in our current study.

Mn and Ni diffusion mobilities in the FCC Mn–Ni alloys have been examined separately by Bae et al. [26], Zhang et al. [29], and Zhu et al. [8]. Bae et al. [26] performed the earliest assessment of diffusion mobilities. However, the subsequent update of the thermodynamic description of the Mn–Ni binary changes the thermodynamic factor, which makes the mobilities by Bae et al. [26] unreliable. Based on the latest thermodynamic description by Liu [5], Zhang et al. [29] reassessed the diffusion mobilities of the FCC Mn–Ni system, which could reproduce diffusion coefficient data from the literature. Recently, Zhu et al. [8] determined interdiffusivities with the diffusion-couple method to support their mobility assessment. A preferable agreement was achieved between the

computational and experimental outcomes. Thus, the mobility parameters by Zhu et al. [8] were employed herein.

In the case of the Fe–Mn–Ni ternary, the experimental diffusion coefficients and mobility description were still lacking. To this end, our current study measured the 1373 K interdiffusivities and assessed the ternary mobility parameters for the FCC phase.

3. Experiments

To measure the phase equilibria below 1073 K for the Fe–Mn–Ni ternary, we designed and annealed four ternary alloys at 923, 973, or 1023 K. Their chemical compositions are listed in Table 1, along with the temperatures and durations of heat treatment. Seven diffusion couples were envisaged for acquiring composition–distance profiles, followed by extraction of interdiffusion coefficients, including four in the Fe-rich part and three in the Ni-rich part, as presented in Table 2. Source materials used herein were Fe (99.99 wt.%), Mn (99.95 wt.%), and Ni (99.999 wt.%). The melting of alloys was accomplished inside an arc-melting furnace in an Ar atmosphere. The ingots were remelted six times. To further ensure chemical homogeneity, a 7-day annealing of ingots was implemented at 1373 K, followed by sectioning of ingots into blocks (7 mm × 7 mm × 7 mm). After encapsulation in quartz capsules, those blocks used for measuring phase equilibria were annealed at temperatures specified in Table 1. As for the diffusion couple experiments, a mirror-like surface was required following the grinding and polishing treatments. The next step was the binding of two end members in a diffusion couple together via a Mo clamp, as shown in Figure 1. Prior to 96 h of annealing at 1373 K, each diffusion-couple assembly was encapsulated inside a quartz capsule in an Ar atmosphere. After that, the diffusion couples were quenched in water, ground, and subsequently polished. On a JEOL JXA 8900 system, individual phase compositions and the composition–distance profiles were assessed through the electron probe microanalysis (EPMA). The probe current was set at 20 nA, while the acceleration voltage was set at 20 kV.

Table 1. Chemical compositions and thermal treatment settings for four Fe–Mn–Ni alloys.

Alloy	Composition (wt.%)	Temperature (K)	Time (Days)
1	Fe–4Mn–4Ni	923	70
		973	60
2	Fe–8Mn–2Ni	923	70
		973	60
3	Fe–2Mn–2Ni	1023	50
		973	70
4	Fe–2Mn–4Ni	973	70

Table 2. Compositions and heat-treatment conditions of diffusion couples.

Diffusion Couple	Composition (at.%)	Temperature (K)	Time (Hours)
F1	Fe/Fe–15.42Mn–83.04Ni	1373	96
F2	Fe/Fe–15.36Mn–14.09Ni	1373	96
F3	Fe–14.46Mn/Fe–18.26Ni	1373	96
F4	Fe–14.50Mn/Fe–49.33Ni	1373	96
N1	Ni/Fe–14.52Mn	1373	96
N2	Ni–21.35Fe/Ni–15.74Mn	1373	96
N3	Ni–49.85Fe/Ni–16.46Mn	1373	96

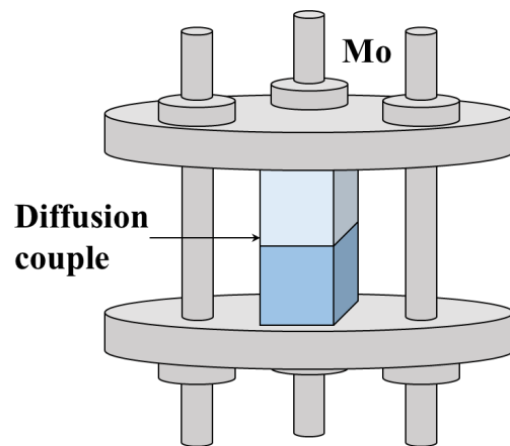


Figure 1. Schematic diagram of the Mo clamp.

4. Modeling

4.1. Thermodynamic Models

The Fe–Mn–Ni ternary has a total of nine phases: liquid, FCC, BCC, α Mn, β Mn, ordered L_{12} , L_{10} and B2, and $MnNi_2$. Zhang et al. [2] established appropriate thermodynamic models for these phases. For the elucidation of the liquid, FCC, BCC, α Mn, and β Mn phases, we adopted the substitutional solution model. The L_{10} phase was depicted with the two-sublattice model, whereas the L_{12} and B2 phases were described with the order/disorder model. FCC and BCC are the disordered parts of the L_{12} and B2 phases, respectively. Based on the order/disorder model, in case the atoms exhibit disordered distribution, the contribution to Gibbs energy resulting from chemical ordering will become zero. When the phase is ordered, the ordered part of Gibbs energy is added. Moreover, Zhang et al. [2] considered the influence of binary reciprocal parameters in the Mn–Ni binary on the L_{12} phase Gibbs energy in ternary alloys. Therefore, identical thermodynamic models were used in our current work. The entire thermodynamic models were grounded on compound energy formalism (CEF) [30]. The Gibbs descriptions for pure elements were taken from Dinsdale [31]. Thermodynamic model parameters for the Fe–Mn, Fe–Ni, and Mn–Ni systems were obtained from Huang [3] and Djurovic et al. [15], Wang [6], and Liu [5], respectively. By extrapolating the sub-binary descriptions, it was found that only the interaction parameters for the β Mn phase require optimization, as in the study by Zhang et al. [2]. Thus, only the β Mn phase thermodynamic model is presented here. Based on the substitutional solution model, the Gibbs energy for β Mn phase can be calculated by using

$$G_m^{\beta Mn} = x_{Fe} {}^{\circ}G_{Fe}^{\beta Mn} + x_{Mn} {}^{\circ}G_{Mn}^{\beta Mn} + x_{Ni} {}^{\circ}G_{Ni}^{\beta Mn} + RT(x_{Fe} \ln x_{Fe} + x_{Mn} \ln x_{Mn} + x_{Ni} \ln x_{Ni}) + x_{Fe} x_{Mn} L_{Fe,Mn}^{\beta Mn} + x_{Fe} x_{Ni} L_{Fe,Ni}^{\beta Mn} + x_{Mn} x_{Ni} L_{Mn,Ni}^{\beta Mn} \quad (1)$$

where x_i stands for the molar fraction of Fe, Mn, or Ni; R and T denote the gas constant and absolute temperature, respectively; ${}^{\circ}G_i^{\beta Mn}$ represents the molar Gibbs energy of pure Fe, Mn, or Ni; and L represents the binary interaction parameters. The terms $L_{Fe,Mn}^{\beta Mn}$ and $L_{Mn,Ni}^{\beta Mn}$ were taken from the binary descriptions [3,5], whereas $L_{Fe,Ni}^{\beta Mn}$ was optimized in our current work. Noticeably, no ternary interaction parameter was introduced in the present study.

4.2. Diffusion Mobility Modeling

The diffusion mobility model, which was originated by Andersson and Ågren [32], was later modified by Jönsson [33]. The computational expression for mobility is

$$M_i = M_i^0 \exp\left(\frac{-Q_i}{RT}\right) \frac{1}{RT} {}^{mg}\Gamma = \frac{1}{RT} \exp\left(\frac{-Q_i + RT \ln M_i^0}{RT}\right) {}^{mg}\Gamma \quad (2)$$

where M_i^0 refers to the frequency factor; Q_i denotes activation energy; and ${}^{mg}\Gamma$ represents a factor considering ferromagnetic ordering. Note that this is ignored for the FCC phase. Q_i and $RT\ln M_i^0$ stand for the temperature- and composition-reliant properties, respectively, which are expressed using Redlich–Kister polynomials [34].

$$\Phi_i = \sum_p x_p \Phi_i^p + \sum_p \sum_{q>p} x_p x_q \left[\sum_{r=0,1,2,\dots} {}^r\Phi_i^{p,q} (x_p - x_q)^r \right] + \sum_p \sum_{p>q} \sum_{t>q} x_p x_q x_t \left[\sum_s v_{pqt}^s \Phi_i^{p,q,t} \right], \quad (s = p, q, t) \quad (3)$$

where x_p and Φ_i^p are the mole fraction and Φ_i value for i in species p , respectively, and ${}^r\Phi_i^{p,q,t}$, ${}^s\Phi_i^{p,q,t}$ refer separately to the binary and ternary interaction. The term v_{pqt}^s was given by $v_{pqt}^s = x_s + (1 - x_p - x_q - x_t)/3$.

Computation of the self-, impurity, tracer, and interdiffusion coefficients was possible based on the mobilities. For instance, the tracer diffusivity D_i^* can be calculated using the Einstein relation:

$$D_i^* = RTM_i \quad (4)$$

The interdiffusion coefficient \tilde{D}_{pq}^n was calculated using

$$\tilde{D}_{pq}^n = \sum_i (\delta_{ip} - x_p) x_i M_i \left(\frac{\partial \mu_i}{\partial x_q} - \frac{\partial \mu_i}{\partial x_n} \right) \quad (5)$$

where n is the dependent species, and δ_{ip} stands for Kronecker delta. Its value is 1 if $i = p$, whereas it is 0 if not. μ_i denotes chemical potential obtained from the thermodynamic elucidation of the corresponding system.

5. Results and Discussion

5.1. Thermodynamic Assessment

Four investigated alloys after annealing were subjected to phase composition measurement by using EPMA, and the results are shown in Table 3. Figure 2 depicts a typical backscattered secondary electron (BSE) micrograph for the annealed alloys. All of the four alloys exhibited a two-phase microstructure of FCC + BCC. The light gray region indicates the FCC phase, while the dark gray region indicates the BCC phase. Composition analysis revealed that within a temperature scope of 923–1023 K, the FCC phase contained significantly more alloying elements when compared to the BCC phase. Additionally, tie-lines between the two phases can be determined, as illustrated in Figure 3f–h.

Table 3. Phase composition analysis for four Fe–Mn–Ni alloys.

Alloy	Temperature (K)	Phase Composition (wt.%)			
		BCC		FCC	
		Mn	Ni	Mn	Ni
1	923	2.07	2.08	4.72	4.96
	973	1.35	1.88	4.09	4.15
2	923	2.61	0.91	7.82	1.96
	973	1.41	1.72	4.10	3.90
3	1023	1.10	1.24	2.52	2.72
	973	1.02	2.31	2.87	5.34

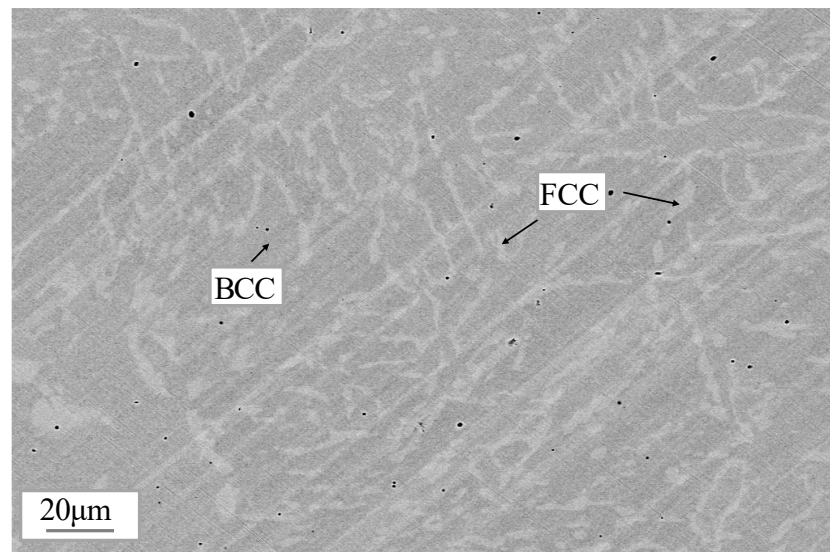


Figure 2. BSE micrograph of Alloy 3 annealed at 973 K for 60 days.

Based on the Fe–Mn system by Huang [3] and Djurovic et al. [15], Fe–Ni by Wang [6], and Mn–Ni by Liu [5], available experimental documents were exploited to assess the Fe–Mn–Ni system. As in the study by Zhang et al. [2], only one interaction parameter was introduced, that is, ${}^0L_{\text{Fe,Ni}}^{\beta\text{Mn}} = -12,000$. All thermodynamic parameters for the Fe–Mn–Ni system are summarized in Table 4. After computing the isothermal sections in the Fe-rich part from 923 to 1792 K, they were contrasted with the experimental measurements in our present study and from literature [2,35], as shown in Figure 3, and also with the computations based on the thermodynamic model parameters from Zhang et al. [2]. Kundrat [35] measured the liquid–FCC or BCC phase equilibria over a temperature range between 1758 and 1792 K, whereas Zhang et al. [2] explored the 1073 K phase equilibria over the whole composition range. As is clear from Figure 3, the two assessments coincided well with the experimental data. However, because of the different Fe–Ni descriptions used in the two assessments, the present model parameters reproduced the phase equilibria at 1758 K, whereas Zhang et al.’s [2] models described the equilibria at 1778 K, a temperature difference of only 20 K. It was very difficult to find agreement between these data simultaneously unless we used a very large temperature-dependent parameter, which is undesirable. Additionally, although the agreement of the phase equilibria at 923 K in Figure 3h is not good, our current computation is acceptable considering the good description of those at 1023 and 973 K. Comparisons are made between the calculated isoplethal sections of the ternary and the experimental outcomes [2,35,36], as displayed in Figure 4. Parravano [36] obtained the phase transformation temperatures for 36 Fe–Mn–Ni alloys over the whole composition range. Kundrat [35] estimated the liquidus temperatures of 23 Fe–Mn–Ni alloys through differential thermal analysis. By using differential thermal analysis, Zhang et al. [2] measured the phase transformation temperatures of seven Fe–Mn–Ni alloys. Clearly, the experimental findings in the literature [2,35,36] are consistent with each other. The calculated results using the model parameters in our current study closely approximate those by Zhang et al. [2]. Both calculations conform reasonably to the experimental outcomes. Figure 5 shows the calculated liquidus projection and liquidus isolines as well as the measured liquidus temperatures [36]. A good agreement is obtained. Based on the comprehensive comparison, it is believed that our thermodynamic elucidation of Fe–Mn–Ni ternary can predict the phase stabilities over a wide temperature range. Moreover, it can provide reliable thermodynamic factors for diffusion simulations.

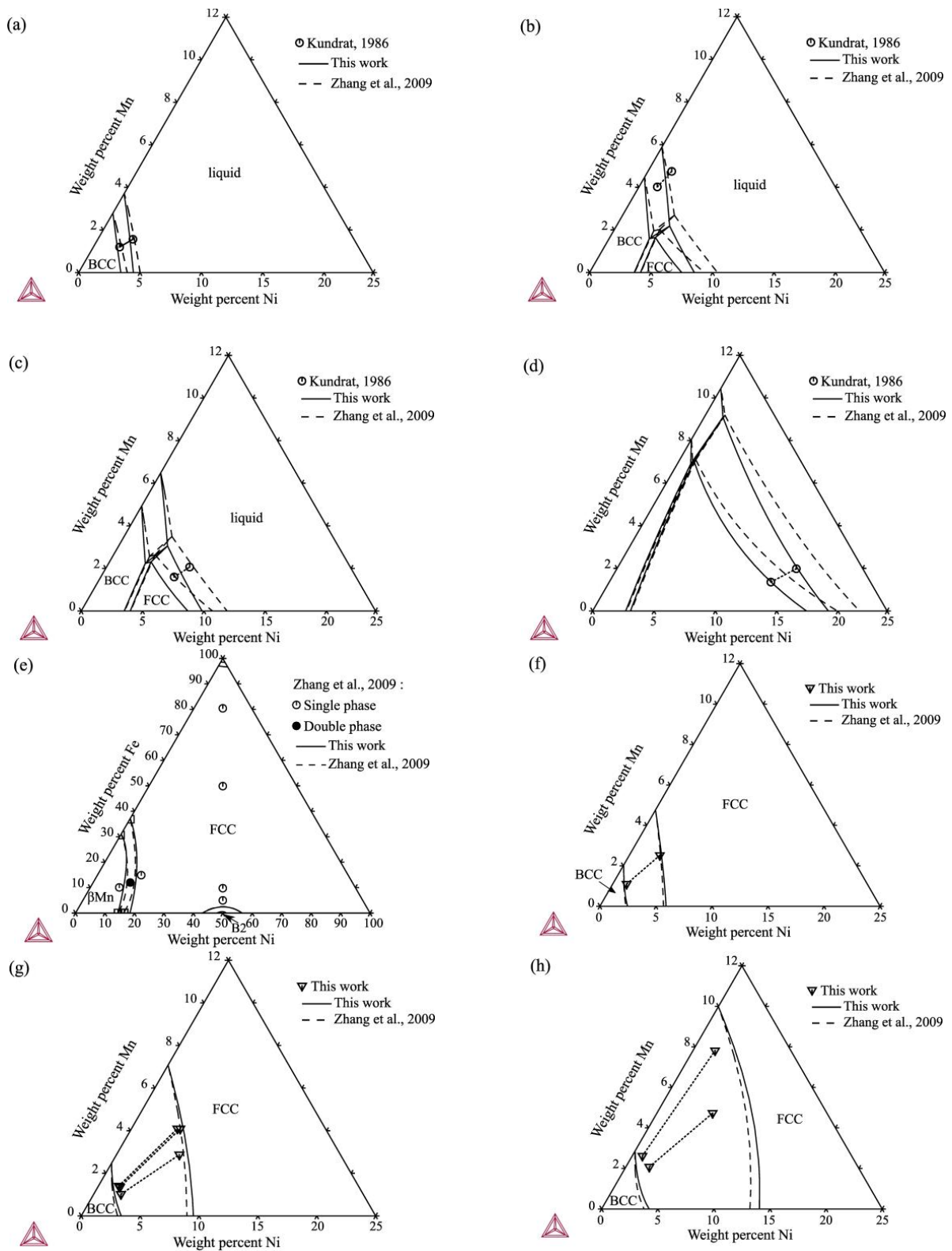


Figure 3. Calculated isothermal sections for Fe–Mn–Ni ternary at (a) 1792 K, (b) 1781 K, (c) 1778 K, (d) 1758 K, (e) 1073 K, (f) 1023 K, (g) 973 K, and (h) 923 K. The experimental data are from this work and Refs. [2,35].

Table 4. Thermodynamic parameters of the Fe–Mn–Ni system.

Phase	Thermodynamic Parameters	Refs.
Liquid (Fe,Mn,Ni) ₁	${}^0L_{\text{Fe,Mn}}^{\text{liquid}} = -3950 + 0.489 \times T$	[3]
	${}^1L_{\text{Fe,Mn}}^{\text{liquid}} = 1145$	[3]
	${}^0L_{\text{Fe,Ni}}^{\text{liquid}} = -16,777 + 2.899 \times T$	[6]
	${}^1L_{\text{Fe,Ni}}^{\text{liquid}} = 10,374 - 2.2796 \times T$	[6]
	${}^2L_{\text{Fe,Ni}}^{\text{liquid}} = -1256.07$	[6]
	${}^0L_{\text{Mn,Ni}}^{\text{liquid}} = -44,423 - 2.35 \times T$	[5]
	${}^1L_{\text{Mn,Ni}}^{\text{liquid}} = 11,941 - 6.85 \times T$	[5]
	BCC (Fe,Mn,Ni) ₁	${}^0L_{\text{Fe,Mn}}^{\text{bcc}} = -2759 + 1.237 \times T$
${}^0T_{\text{Fe,Mn}}^{\text{bcc}} = 123$		[3]
${}^0L_{\text{Fe,Ni}}^{\text{bcc}} = -5018 - 0.8664 \times T$		[6]
${}^1L_{\text{Fe,Ni}}^{\text{bcc}} = 7726 - 4.00 \times T$		[6]
${}^0T_{\text{Fe,Ni}}^{\text{bcc}} = -1000$		[6]
${}^1T_{\text{Fe,Ni}}^{\text{bcc}} = 1500$		[6]
${}^0\beta_{\text{Fe,Ni}}^{\text{bcc}} = -0.5$		[6]
${}^1\beta_{\text{Fe,Ni}}^{\text{bcc}} = 3.5$		[6]
FCC (Fe,Mn,Ni) ₁	${}^0L_{\text{Fe,Mn}}^{\text{fcc}} = -7762 + 3.865 \times T$	[3]
	${}^1L_{\text{Fe,Mn}}^{\text{fcc}} = -259$	[3]
	${}^0T_{\text{Fe,Mn}}^{\text{fcc}} = -2282$	[3]
	${}^1T_{\text{Fe,Mn}}^{\text{fcc}} = -2068$	[3]
	${}^0L_{\text{Fe,Ni}}^{\text{fcc}} = -14,804 + 2.705 \times T$	[6]
	${}^1L_{\text{Fe,Ni}}^{\text{fcc}} = 12,459 - 3.37 \times T$	[6]
	${}^2L_{\text{Fe,Ni}}^{\text{fcc}} = -1554.55$	[6]
	${}^0T_{\text{Fe,Ni}}^{\text{fcc}} = 2200$	[6]
	${}^1T_{\text{Fe,Ni}}^{\text{fcc}} = -700$	[6]
	${}^2T_{\text{Fe,Ni}}^{\text{fcc}} = -800$	[6]
	${}^0\beta_{\text{Fe,Ni}}^{\text{fcc}} = 10$	[6]
	${}^1\beta_{\text{Fe,Ni}}^{\text{fcc}} = 8$	[6]
	${}^2\beta_{\text{Fe,Ni}}^{\text{fcc}} = 4$	[6]
	${}^0L_{\text{Mn,Ni}}^{\text{fcc}} = -20,456 - 11.79 \times T$	[5]
${}^1L_{\text{Mn,Ni}}^{\text{fcc}} = 15,582 - 8.49 \times T$	[5]	
${}^0T_{\text{Mn,Ni}}^{\text{fcc}} = -3171.1978$	[5]	
${}^1T_{\text{Mn,Ni}}^{\text{fcc}} = -4317.7323$	[5]	
α Mn (Fe,Mn,Ni) ₁	${}^0L_{\text{Fe,Mn}}^{\text{cbcc}} = -10,184$	[3]
	${}^0L_{\text{Mn,Ni}}^{\text{cbcc}} = 40,445.791$	[5]
	${}^1L_{\text{Mn,Ni}}^{\text{cbcc}} = -49,309 - 21.047 \times T$	[5]
β Mn (Fe,Mn,Ni) ₁	${}^0L_{\text{Fe,Mn}}^{\text{cub}} = -11,518 + 2.819 \times T$	[3]
	${}^0L_{\text{Fe,Ni}}^{\text{cub}} = -12,000$	This work
	${}^0L_{\text{Mn,Ni}}^{\text{cub}} = -6586 - 20.215 \times T$	[5]
HCP (Fe,Mn,Ni) ₁	${}^0L_{\text{Fe,Mn}}^{\text{hcp}} = -5582 + 3.865 \times T$	[15]
	${}^1L_{\text{Fe,Mn}}^{\text{hcp}} = 273$	[15]
B2 (Fe,Mn,Ni) _{0.5} (Fe,Mn,Ni) _{0.5}	${}^0G_{\text{Fe:Fe}}^{\text{B2}} = {}^0G_{\text{Mn:Mn}}^{\text{B2}} = {}^0G_{\text{Ni:Ni}}^{\text{B2}} = 0$	This work
	${}^0G_{\text{Fe:Ni}}^{\text{B2}} = {}^0G_{\text{Ni:Fe}}^{\text{B2}} = -2087.3357$	[6]
	${}^0G_{\text{Mn:Ni}}^{\text{B2}} = {}^0G_{\text{Ni:Mn}}^{\text{B2}} = -24,341.195 + 4.358 \times T$	[5]

Table 4. Cont.

Phase	Thermodynamic Parameters	Refs.
L1 ₂	GFE3NI = 13,905.8374	[6]
(Fe,Mn,Ni) _{0.75} (Fe,Mn,Ni) _{0.25}	GFENI3 = −16,978 + 15.187 × T	[6]
	GFE2NI2 = 0	[6]
	LFENI0 = −458.90	[6]
	GMN3NI = −20,080.5831	[5]
	GMNNI3 = −21,016.3924	[5]
	GMN2NI2 = −30,156.6806	[5]
	LMNNIF0 = −20,456 − 11.79 × T	[5]
	LMNNIF1 = +15,582 − 8.49 × T	[5]
	LRMNNI = −6829	[5]
	GFE2MNNI = 0.666667GFENI3 + 0.333333GMNNI3 + 10,000	This work
	GFEMN2NI = 0.333333GFENI3 + 0.666667GMNNI3	This work
	GFEMNNI2 = 0.666667GFENI3 + 0.666667GMNNI3	This work
	⁰ G _{Fe:Fe} ^{L1₂} = ⁰ G _{Mn:Mn} ^{L1₂} = ⁰ G _{Ni:Ni} ^{L1₂} = 0	This work
	⁰ G _{Fe:Ni} ^{L1₂} = GFE3NI	[6]
	⁰ G _{Ni:Fe} ^{L1₂} = GFENI3	[6]
	⁰ L _{Fe,Ni:Fe} ^{L1₂} = −1.5GFENI3 + 1.5GFE2NI2 + 1.5GFE3NI	[6]
	¹ L _{Fe,Ni:Fe} ^{L1₂} = 0.5GFENI3 − 1.5GFE2NI2 + 1.5GFE3NI	[6]
	⁰ L _{Fe,Ni:Ni} ^{L1₂} = 1.5GFENI3 + 1.5GFE2NI2 − 1.5GFE3NI	[6]
	¹ L _{Fe,Ni:Ni} ^{L1₂} = −1.5GFENI3 + 1.5GFE2NI2 − 0.5GFE3NI	[6]
	⁰ L _{Fe,Ni:*} ^{L1₂} = 3LFENI0	[6]
	¹ L _{Fe,Ni:*} ^{L1₂} = 3LFENI1	[6]
	⁰ L _{*:Fe,Ni} ^{L1₂} = LFENI0	[6]
	¹ L _{*:Fe,Ni} ^{L1₂} = LFENI1	[6]
	⁰ L _{Mn,Ni:Mn} ^{L1₂} = −1.5GMNNI3 + 1.5GMN2NI2 + 1.5GMN3NI	[5]
	¹ L _{Mn,Ni:Mn} ^{L1₂} = 0.5GMNNI3 − 1.5GMN2NI2 + 1.5GMN3NI	[5]
	⁰ L _{Mn,Ni:Ni} ^{L1₂} = 1.5GMNNI3 + 1.5GMN2NI2 − 1.5GMN3NI	[5]
	¹ L _{Mn,Ni:Ni} ^{L1₂} = −1.5GMNNI3 + 1.5GMN2NI2 − 0.5GMN3NI	[5]
	⁰ L _{Mn,Ni:*} ^{L1₂} = 0.75LRMNNI	[5]
	¹ L _{Mn,Ni:*} ^{L1₂} = 0	[5]
	² L _{Mn,Ni:*} ^{L1₂} = −0.75LRMNNI	[5]
	⁰ L _{Mn,Ni:Mn,Ni} ^{L1₂} = 3LRMNNI	[5]
	⁰ L _{Fe,Mn:Ni} ^{L1₂} = −1.5GFE3NI − 1.5GMN3NI + 1.5GFEMN2NI + 1.5GFE2MNNI	This work
	⁰ L _{Fe,Ni:Mn} ^{L1₂} = −1.5GMNNI3 + 1.5GFEMNNI2 + 1.5GFE2MNNI	This work
	⁰ L _{Mn,Ni:Fe} ^{L1₂} = −1.5GFENI3 + 1.5GFEMNNI2 + 1.5GFEMN2NI	This work
	¹ L _{Fe,Mn:Ni} ^{L1₂} = −0.5GFE3NI + 0.5GMN3NI − 1.5GFEMN2NI + 1.5GFE2MNNI	This work
	¹ L _{Fe,Ni:Mn} ^{L1₂} = 0.5GMNNI3 − 1.5GFEMNNI2 + 1.5GFE2MNNI	This work
	¹ L _{Mn,Ni:Fe} ^{L1₂} = 0.5GFENI3 − 1.5GFEMNNI2 + 1.5GFEMN2NI	This work
	⁰ L _{Fe,Mn,Ni:Fe} ^{L1₂} = GFENI3 − 1.5GFE3NI − 1.5GFEMNNI2 − 1.5GFEMN2NI + 6GFE2MNNI	This work
	⁰ L _{Fe,Mn,Ni:Mn} ^{L1₂} = GMNNI3 − 1.5GMN2NI2 − 1.5GMN3NI − 1.5GFEMNNI2 + 6GFEMN2NI − 1.5GFE2MNNI	This work
	⁰ L _{Fe,Mn,Ni:Ni} ^{L1₂} = −1.5GFENI3 + GFE3NI − 1.5GMNNI3 − 1.5GMN2NI2 + GMN3NI + 6GFEMNNI2 − 1.5GFEMN2NI − 1.5GFE2MNNI	This work
	⁰ L _{Fe,Ni:Mn,Ni} ^{L1₂} = ⁰ L _{Mn,Ni:Fe,Ni} ^{L1₂} = ⁰ L _{Fe,Mn:Mn,Ni} ^{L1₂} = ⁰ L _{Mn,Ni:Fe,Mn} ^{L1₂} = 0.75LRMNNI	This work
	⁰ L _{Fe,Mn:Fe,Ni} ^{L1₂} = ⁰ L _{Fe,Ni:Fe,Mn} ^{L1₂} = 0.375LRMNNI	This work

Table 4. Cont.

Phase	Thermodynamic Parameters	Refs.
$L1_0$	${}^0G_{Mn:Mn}^{L1_0} - {}^0G_{Mn:Mn}^{fcc} = 10$	[5]
$(Mn,Ni)_{0.5}(Mn,Ni)_{0.5}$	${}^0G_{Ni:Ni}^{L1_0} - {}^0G_{Ni:Ni}^{fcc} = 10$	[5]
	${}^0G_{Mn:Ni}^{L1_0} - 0.5{}^0G_{Mn:Mn}^{fcc} - 0.5{}^0G_{Ni:Ni}^{fcc}$ $= -10 - 0.25GMN3NI + 0.625GMN2NI2$ $- 0.25GMN3NI - 0.375LRMNNI + 0.25LMNINF0$	[5]
	${}^0G_{Ni:Mn}^{L1_0} - 0.5{}^0G_{Mn:Mn}^{fcc} - 0.5{}^0G_{Ni:Ni}^{fcc}$ $= -10 - 0.25GMN3NI + 0.625GMN2NI2$ $- 0.25GMN3NI - 0.375LRMNNI + 0.25LMNINF0$	[5]
	${}^0L_{Mn,Ni:Mn}^{L1_0} = {}^0L_{Mn:Mn,Ni}^{L1_0}$ $= 0.3125GMN3NI - 1.09375GMN2NI2$ $+ 0.8125GMN3NI + 0.15625LRMNNI$ $+ 0.25LMNINF0 + 0.375LMNINF1$	[5]
	${}^1L_{Mn,Ni:Mn}^{L1_0} = {}^1L_{Mn:Mn,Ni}^{L1_0}$ $= 0.375GMN2NI2 - 0.5GMN3NI + 0.375LRMNNI$ $+ 0.125LMNINF1$	[5]
	${}^2L_{Mn,Ni:Mn}^{L1_0} = {}^2L_{Mn:Mn,Ni}^{L1_0}$ $= -0.0625GMN3NI + 0.09375GMN2NI2$ $- 0.0625GMN3NI - 0.15625LRMNNI$	[5]
	${}^0L_{Mn,Ni:Ni}^{L1_0} = {}^0L_{Ni:Mn,Ni}^{L1_0}$ $= 0.8125GMN3NI - 1.09375GMN2NI2$ $+ 0.3125GMN3NI + 0.15625LRMNNI$ $+ 0.25LMNINF0 - 0.375LMNINF1$	[5]
	${}^1L_{Mn,Ni:Ni}^{L1_0} = {}^1L_{Ni:Mn,Ni}^{L1_0}$ $= 0.5GMN3NI - 0.375GMN2NI2 - 0.375LRMNNI$ $+ 0.125LMNINF1$	[5]
	${}^2L_{Mn,Ni:Ni}^{L1_0} = {}^2L_{Ni:Mn,Ni}^{L1_0}$ $= -0.0625GMN3NI + 0.09375GMN2NI2$ $- 0.0625GMN3NI - 0.15625LRMNNI$	[5]
	${}^0L_{Mn,Ni:Mn,Ni}^{L1_0} = 0$	[5]
	${}^1L_{Mn,Ni:Mn,Ni}^{L1_0} = -2.5GMN3NI + 3.75GMN2NI2 - 2.5GMN3NI$ $+ 1.75LRMNNI$	[5]
$MnNi_2$	${}^0G_{Mn:Ni}^{MnNi_2} - {}^0G_{Mn:Mn}^{cbcc} - 2{}^0G_{Ni:Ni}^{fcc} = -27,085 - 5.99 \times T$	[5]
$(Mn,Ni)_1(Ni)_2$	${}^0G_{Ni:Ni}^{MnNi_2} - 3{}^0G_{Ni:Ni}^{fcc} = 15,000$	[5]
	${}^0L_{Mn,Ni:Ni}^{MnNi_2} = -19,871$	[5]

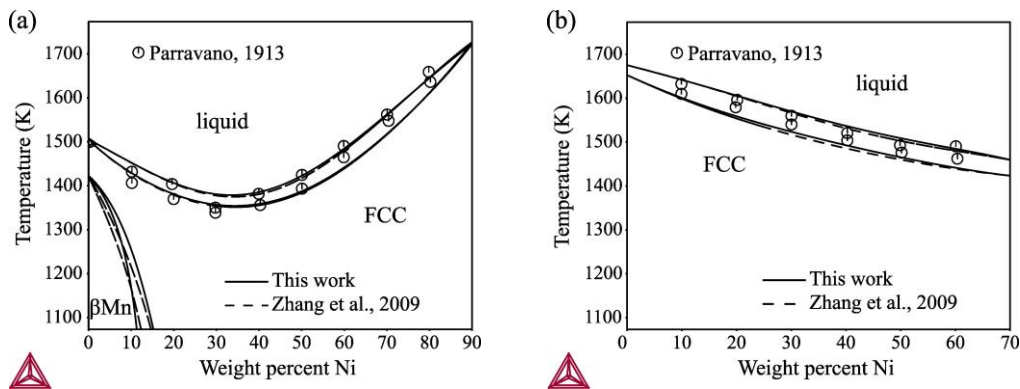


Figure 4. Cont.

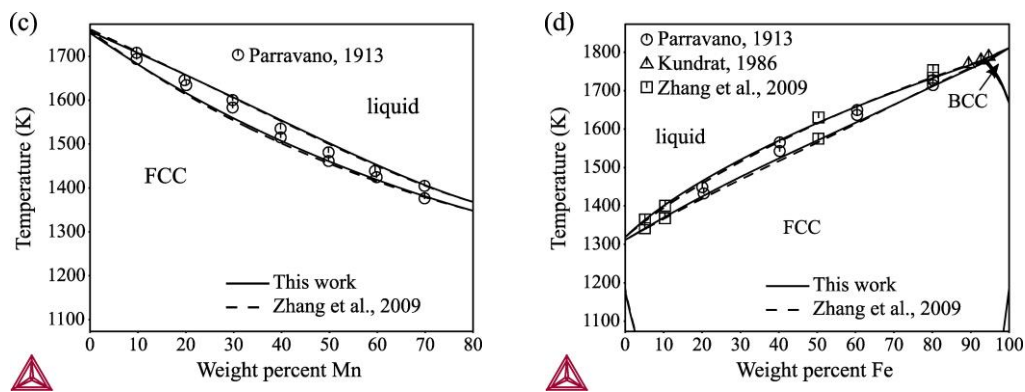


Figure 4. Isoplethal section computations for Fe–Mn–Ni ternary at (a) Fe (10 wt.%), (b) Mn (30 wt.%), (c) Ni (20 wt.%) and (d) $w(\text{Mn})/w(\text{Ni}) = 1$. The experimental data are from Refs. [2,35,36].

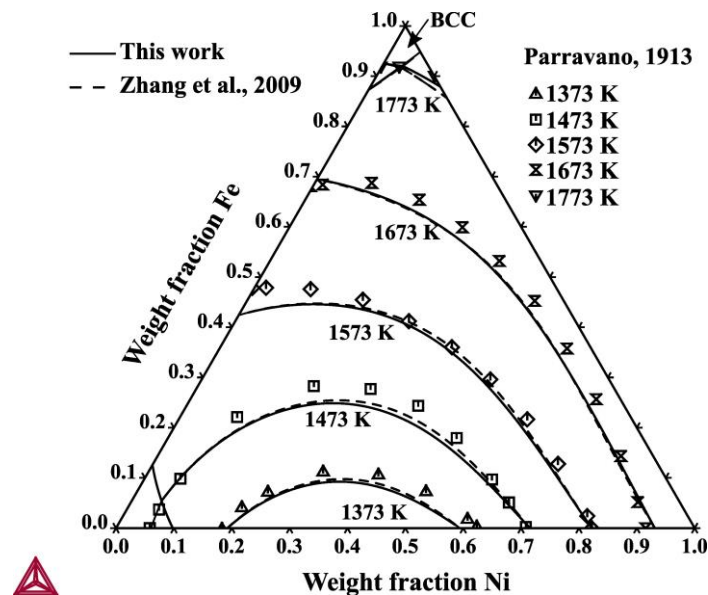


Figure 5. Liquidus projection and iseline computations for Fe–Mn–Ni ternary calculated by using the parameters in this work and from Ref. [2]. The experimental data are from Ref. [36].

5.2. Diffusion Mobility Optimization

A typical backscattered secondary electron (BSE) micrograph for the diffusion couple is depicted in Figure 6. The composition–distance profiles of the diffusion couples were measured using EPMA. Based on the composition–distance profiles, the interdiffusivities in the FCC Fe–Mn–Ni alloys were derived through the Whittle–Green approach [37]. Before that, smoothing of composition–distance profiles was accomplished exploiting error function expansion, i.e., $X(z) = \sum_i a_i \text{erf}(b_i z - c_i) + d_i$, where X denotes composition; z represents distance; and a , b , c and d are the adjustable parameters. The interdiffusion coefficients at the intersections were determined as summarized in Table 5. Note that the dependent component should be chosen during extraction. In fact, the dependent component is selected arbitrarily, despite the presence of preference during practice. Because the Fe-rich and Ni-rich diffusion couples were investigated in our current study, the interdiffusivities were deduced twice, once with Fe as the dependent component and once with Ni as the dependent component. According to our finding, the main interdiffusivities are one order of magnitude greater in the Ni-rich part compared to those in the Fe-rich part, implying quicker diffusion in FCC Ni compared to that in FCC Fe. When Fe is the

dependent component, Mn diffuses faster in contrast to Ni. When Ni is the dependent component, Mn also diffuses faster in contrast to Fe.

Table 5. Experimental interdiffusivities with Fe or Ni as the dependent component for the FCC Fe–Mn–Ni system.

Diffusion Couple	Composition (at%)			Interdiffusion Coefficients ($\times 10^{-15}$ m ² /s)							
	Fe	Mn	Ni	$\tilde{D}_{\text{MnMn}}^{\sim\text{Fe}}$	$\tilde{D}_{\text{MnNi}}^{\sim\text{Fe}}$	$\tilde{D}_{\text{NiMn}}^{\sim\text{Fe}}$	$\tilde{D}_{\text{NiNi}}^{\sim\text{Fe}}$	$\tilde{D}_{\text{FeFe}}^{\sim\text{Ni}}$	$\tilde{D}_{\text{FeMn}}^{\sim\text{Ni}}$	$\tilde{D}_{\text{MnFe}}^{\sim\text{Ni}}$	$\tilde{D}_{\text{MnMn}}^{\sim\text{Ni}}$
F1/F3	81.15	0.83	18.02	3.59	0.02	0.22	2.09	2.77	−0.15	−0.01	3.87
F1/F4	51.26	2.43	46.31	12.11	−0.71	−4.77	6.56	5.02	−1.21	0.60	13.07
F2/F3	89.15	7.05	3.80	2.63	−0.08	−0.11	0.46	−0.05	−3.43	−0.12	2.08
F2/F4	84.45	8.59	6.96	2.90	−0.31	−1.24	1.08	0.60	−1.44	0.53	3.91
F2/N1	83.45	8.94	7.61	2.60	−0.25	−1.61	1.46	1.11	0.03	0.03	3.56
N1/F1	36.86	4.64	58.50	19.70	−3.11	−4.78	12.51	10.62	−7.04	3.84	25.74
N1/N3	28.16	4.80	67.05	17.37	−5.11	−20.42	18.39	12.16	15.64	4.61	22.11
N1/N2	15.29	4.87	79.84	12.08	−4.60	−4.53	14.58	11.72	6.31	5.10	18.32

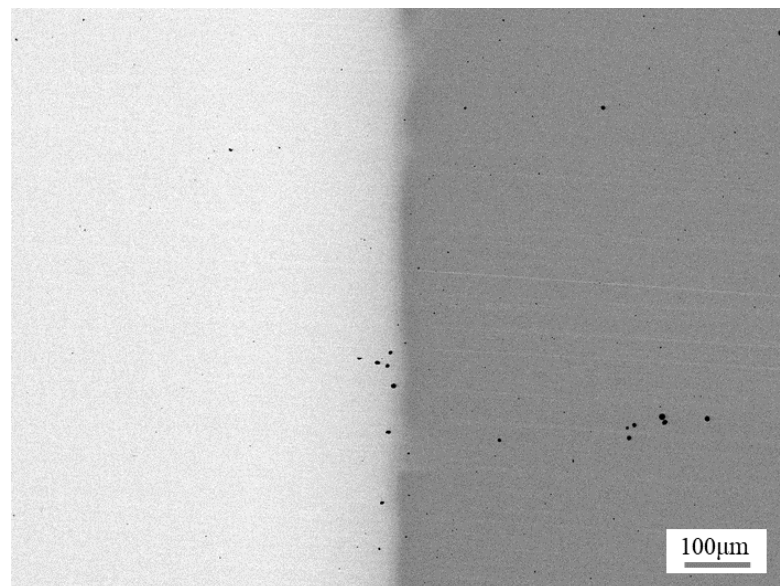


Figure 6. BSE micrograph of N1 diffusion couple annealed at 1373 K for 96 h.

By combining the reliable thermodynamic description and the extracted interdiffusion coefficients, the diffusion mobilities were optimized with the CALPHAD method. The source of self- and impurity diffusion mobilities was Refs. [7,27–29,38]. The binary diffusion mobilities were from the literature, that is, Fe–Mn by Liu et al. [7], Fe–Ni by Wang [6], and Mn–Ni by Zhu et al. [8]. It was found that reproduction of interdiffusion coefficients required only one interaction parameter. The diffusion mobilities are summarized in Table 6. After computing the main interdiffusion coefficients based on our current thermodynamic and mobility descriptions, they were contrasted with extracted ones, as depicted in Figure 7. A reasonable agreement is achieved. Additionally, the agreement of interdiffusivities with Fe as the dependent component is slightly better than that with Ni as the dependent component. This may be due to the fact that the thermodynamic factor in the Fe-rich part is more reliable than that in the Ni-rich part. From Figures 3 and 4, the experimental phase diagram data used to optimize the thermodynamic models mainly concentrate on the Fe-rich part. Hence, there are reasons to believe that the obtained thermodynamic parameters in the Fe-rich part are more reliable than those in the Ni-rich part. For further diffusion mobility confirmation, we calculated composition–distance profiles for the diffusion couples (Figure 8) against the experimental outcomes. According to Figure 8c–e, Fe atoms show

the uphill diffusion behavior in diffusion couples F3, F4, and N1. The calculated diffusion paths were contrasted against the measurements (Figure 9). Several diffusion paths exhibit a clear S-shaped curve, such as the diffusion couple F2, which is attributable to faster Mn diffusion in contrast to Ni. In Figures 8 and 9, a satisfactory agreement was obtained.

Table 6. Diffusion mobilities for the FCC phase in Fe–Mn–Ni ternary.

Mobility	Parameters	Refs.
Mobility of Fe		
Φ_{Fe}^{Fe}	$-286,000 + R \times T \times \text{LN}(7 \times 10^{-5})$	[27]
Φ_{Fe}^{Mn}	$-212,755.85 + R \times T \times \text{LN}(7.6 \times 10^{-6})$	[7]
Φ_{Fe}^{Ni}	$-247,872 + R \times T \times \text{LN}(1.86 \times 10^{-5})$	[28]
$0\Phi_{Fe}^{Fe,Mn}$	$-10,711.05 - 26.32 \times T$	[7]
$1\Phi_{Fe}^{Fe,Mn}$	$+16,312.22$	[7]
$0\Phi_{Fe}^{Fe,Ni}$	$+29,481$	[6]
Mobility of Mn		
Φ_{Mn}^{Fe}	$-246,512.70 + R \times T \times \text{LN}(3.46 \times 10^{-6})$	[7]
Φ_{Mn}^{Mn}	$-212,755.85 + R \times T \times \text{LN}(7.6 \times 10^{-6})$	[7]
Φ_{Mn}^{Ni}	$-261,376.6 + R \times T \times \text{LN}(1.40 \times 10^{-4})$	[29]
$0\Phi_{Mn}^{Fe,Mn}$	$-24,655.58 + 25.32 \times T$	[7]
$1\Phi_{Mn}^{Fe,Mn}$	$-32,017.56$	[7]
$0\Phi_{Mn}^{Mn,Ni}$	$-166,299.65 + 171.27 \times T$	[8]
$0\Phi_{Mn}^{Fe,Ni}$	$+39,000$	This work
Mobility of Ni		
Φ_{Ni}^{Fe}	$-286,000 + R \times T \times \text{LN}(3.2185 \times 10^{-5})$	[27]
Φ_{Ni}^{Mn}	$-212,755.85 + R \times T \times \text{LN}(7.54 \times 10^{-6})$	[29]
Φ_{Ni}^{Ni}	$-276,860 + R \times T \times \text{LN}(8.5 \times 10^{-5})$	[38]
$0\Phi_{Ni}^{Mn,Ni}$	$+234,036.27 - 51.45 \times T$	[8]
$0\Phi_{Ni}^{Fe,Ni}$	$+175,714 - 84.73 \times T$	[6]

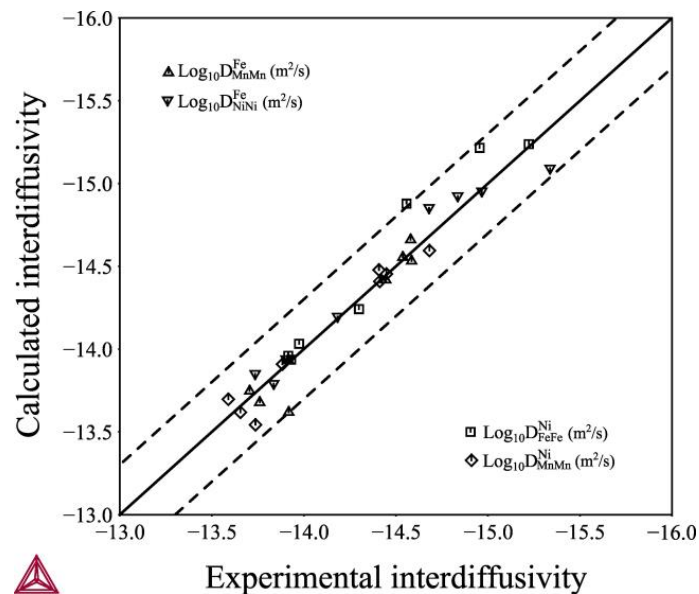


Figure 7. Computed vs. measured 1373 K interdiffusivities in the FCC Fe–Mn–Ni system. The solid line represents a good agreement between the calculated and experimental interdiffusivity, whereas the dashed lines denote the accepted deviation range for the optimization.

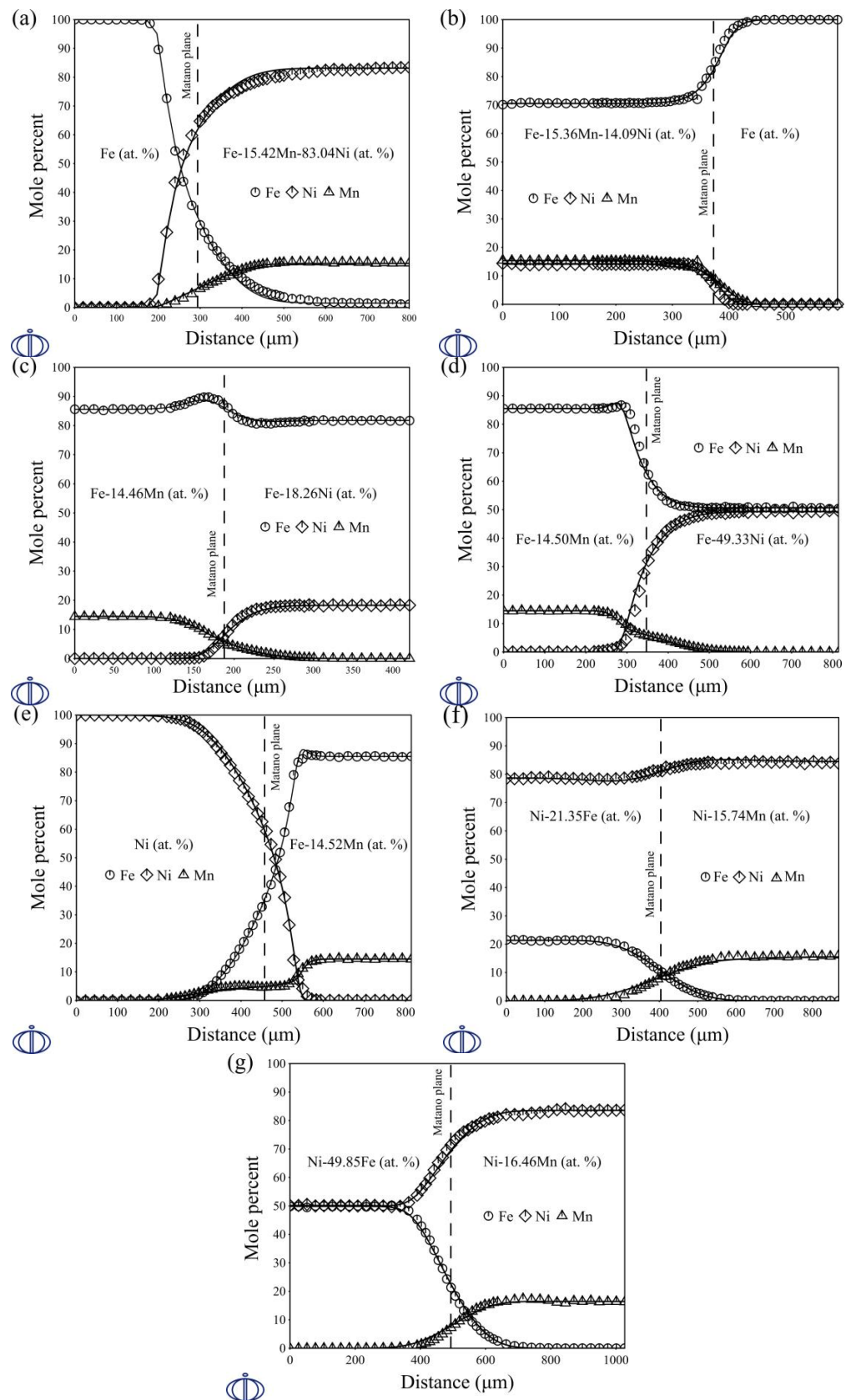


Figure 8. Composition-distance profile simulations vs. measurements for diffusion couples in Fe-Mn-Ni ternary: (a) F1, (b) F2, (c) F3, (d) F4, (e) N1, (f) N2, and (g) N3.

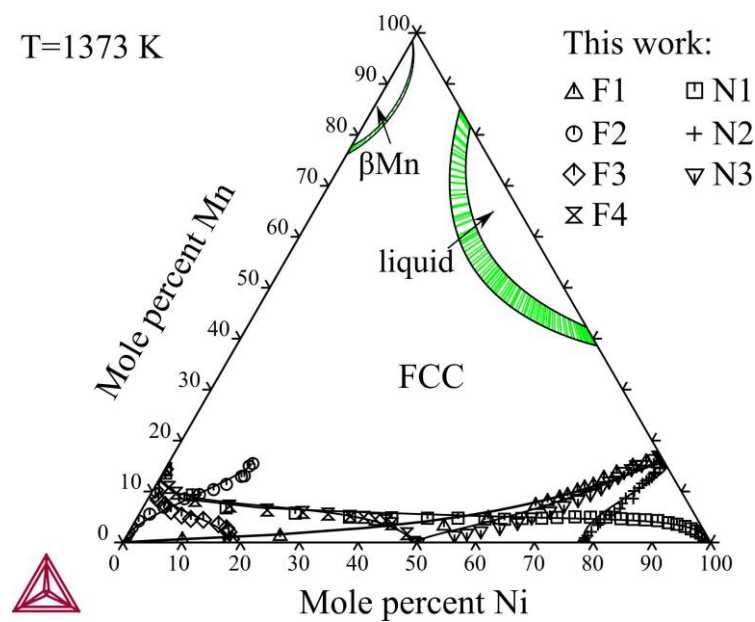


Figure 9. Diffusion path simulations vs. measurements at 1373 K for diffusion couples.

6. Conclusions

A thermodynamic elucidation of the Fe–Mn–Ni ternary was first extrapolated from sub-binary systems. Only one interaction parameter was introduced for the β Mn phase. Phase equilibria at relatively low temperatures measured in our current research confirmed that the extrapolated ternary description is reliable. Apart from enabling reproduction of experimental phase equilibria within a wide temperature scope, the thermodynamic description also provides a reliable thermodynamic factor for the diffusion simulation. The thermodynamic description of the Fe–Mn–Ni ternary was improved based on the updated binary descriptions.

Combined with the diffusion couple method, diffusion mobility optimization was accomplished in the case of the FCC phase in the Fe–Mn–Ni ternary with the utilization of measured interdiffusion coefficients. The interdiffusivity computations based on diffusion mobilities coincided preferably with those obtained using the Whittle–Green approach. The composition–distance profiles were reproduced satisfactorily for the diffusion couples, and so were the diffusion paths. Through holistic comparison of computed diffusion data with experimental ones, the present diffusion mobilities were verified. The present study fills the gap in diffusion mobility for the FCC Fe–Mn–Ni ternary.

In addition, by using the self-consistent thermodynamic and kinetic model parameters obtained in the present study, it is promising to establish the thermodynamic and mobility database for medium-Mn steels and then to predict the austenite transformation behavior during intercritical annealing.

Author Contributions: M.W.: Methodology, Writing—original draft. G.F.: Writing—review and editing. C.M.: Visualization. Y.M.: Investigation. T.L.: Formal analysis. W.Z.: Supervision, Writing—review and editing. J.W.: Writing—review and editing. All authors have read and agreed to the published version of the manuscript.

Funding: This work was supported by the National Natural Science Foundation of China (Grant No. 51901124 and 62273220), the Young Elite Scientists Sponsorship Program of the China Association for Science and Technology (Grant No. YESS20210357). WZ appreciates the financial support from the open foundation of Guangxi Key Laboratory of Information Materials, Guilin University of Electronic Technology (Grant No. 211009-K), State Key Laboratory of Advanced Special Steel, Shanghai Key Laboratory of Advanced Ferrometallurgy, and the Science and Technology Commission of Shanghai Municipality (No. 19DZ2270200).

Data Availability Statement: The data that support this study will be available on request.

Conflicts of Interest: The authors declare no conflict of interest.

References

1. Andersson, J.O.; Helander, T.; Höglund, L.; Shi, P.; Sundman, B. Thermo-Calc & DICTRA, computational tools for materials science. *Calphad* **2002**, *26*, 273–312.
2. Zhang, L.; Xu, H.; Liu, S.; Liu, Y.; Zheng, F.; Dupin, N.; Zhou, H.; Tang, C. Phase equilibria and thermal analysis in the Fe–Mn–Ni system. *Int. J. Mater. Res.* **2009**, *100*, 160–175. [[CrossRef](#)]
3. Huang, W. An assessment of the Fe–Mn system. *Calphad* **1989**, *13*, 243–252. [[CrossRef](#)]
4. Servant, C.; Sundman, B.; Lyon, O. Thermodynamic assessment of the Cu–Fe–Ni system. *Calphad* **2001**, *25*, 79–95. [[CrossRef](#)]
5. Liu, S. Order-Disorder Phase Transition, Phase Diagram Topological Relationship and Its Application in Solidification Process of Aluminum Alloy. Ph.D. Thesis, Central South University, Changsha, China, 2010.
6. Wang, J. Thermodynamic and Diffusion Kinetic Studies of Key Phases in the Co–Al–Fe–Ni System. Ph.D. Thesis, Shanghai University, Shanghai, China, 2020.
7. Liu, Y.; Zhang, L.; Du, Y.; Yu, D.; Liang, D. Atomic mobilities, uphill diffusion and proeutectic ferrite growth in Fe–Mn–C alloys. *Calphad* **2009**, *33*, 614–623. [[CrossRef](#)]
8. Zhu, N.; Xu, X.; Lu, X.-G.; He, Y.; Zhang, J.; Jiang, H. Experimental and computational study of diffusion mobilities for fcc Ni–Cu–Mn alloys. *Calphad* **2016**, *54*, 97–106. [[CrossRef](#)]
9. Kaufman, L. Coupled phase diagrams and thermochemical data for transition metal binary systems-III. *Calphad* **1978**, *2*, 117–146. [[CrossRef](#)]
10. Huang, W. An assessment of the Fe–Mn system. *Calphad* **1987**, *11*, 183–186. [[CrossRef](#)]
11. Lee, B.-J.; Lee, D.N. A thermodynamic study on the Mn–C and Fe–Mn systems. *Calphad* **1989**, *13*, 345–354.
12. Witusiewicz, V.T.; Sommer, F.; Mittemeijer, E.J. Reevaluation of the Fe–Mn phase diagram. *J. Phase Equilibria Diffus.* **2004**, *25*, 346–354. [[CrossRef](#)]
13. Witusiewicz, V.T.; Sommer, F.; Mittemeijer, E.J. Enthalpy of formation and heat capacity of Fe–Mn alloys. *Metall. Mater. Trans. B* **2003**, *34*, 209–223. [[CrossRef](#)]
14. Nakano, J.; Jacques, P.J. Effects of the thermodynamic parameters of the hcp phase on the stacking fault energy calculations in the Fe–Mn and Fe–Mn–C systems. *Calphad* **2010**, *34*, 167–175. [[CrossRef](#)]
15. Djurovic, D.; Hallstedt, B.; Von Appen, J.; Dronskowski, R. Thermodynamic assessment of the Fe–Mn–C system. *Calphad* **2011**, *35*, 479–491. [[CrossRef](#)]
16. Cotes, S.M.; Guillermet, A.F.; Sade, M. Fcc/hcp martensitic transformation in the Fe–Mn system: Part II. Driving force and thermodynamics of the nucleation process. *Metall. Mater. Trans. A* **2004**, *35*, 83–91. [[CrossRef](#)]
17. Byeong-Joo, L. Revision of thermodynamic descriptions of the Fe–Cr and Fe–Ni liquid phases. *Calphad* **1993**, *17*, 251–268. [[CrossRef](#)]
18. Xing, Z.S.; Gohil, D.D.; Dinsdale, A.T.; Chart, T. *National Physical Laboratory DMA (A) 103*; National Physical Laboratory: London, UK, 1985.
19. Cacciamani, G.; Dinsdale, A.; Palumbo, M.; Pasturel, A. The Fe–Ni system: Thermodynamic modelling assisted by atomistic calculations. *Intermetallics* **2010**, *18*, 1148–1162. [[CrossRef](#)]
20. Franke, P.; Seifert, H.J. The influence of magnetic and chemical ordering on the phase diagram of Cr–Fe–Ni. *Calphad* **2011**, *35*, 148–154. [[CrossRef](#)]
21. Ohnuma, I.; Shimenouchi, S.; Omori, T.; Ishida, K.; Kainuma, R. Experimental determination and thermodynamic evaluation of low-temperature phase equilibria in the Fe–Ni binary system. *Calphad* **2019**, *67*, 101677. [[CrossRef](#)]
22. Miettinen, J. Thermodynamic solution phase data for binary Mn-based systems. *Calphad* **2001**, *25*, 43–48. [[CrossRef](#)]
23. Guo, C.; Du, Z. Thermodynamic optimization of the Mn–Ni system. *Intermetallics* **2005**, *13*, 525–534. [[CrossRef](#)]
24. Frank, P. An assessment of the ordered phases in Mn–Ni using two- and four-sublattice models. *Int. J. Mater. Res.* **2007**, *98*, 954–960. [[CrossRef](#)]
25. Ding, L. Experimental Investigation of Phase Equilibria and Interdiffusion Coefficients in Ni–Mn System: A Thesis Submitted in Partial Fulfillment of the Requirements for the Degree of. Master of Science. Master’s Thesis, University of Wisconsin–Madison, Madison, WI, USA, 2001.
26. Bae, J.S.; Yu, J.H.; Lee, B.-J.; Lee, H.M. Assessment of the mobility of Mn in the Fe–Mn and Ni–Mn binary system. *Z. Met.* **2000**, *91*, 672–674. [[CrossRef](#)]
27. Jönsson, B. Mobilities in Fe–Ni alloys—Assessment of the mobilities of Fe and Ni in fcc Fe–Ni alloys. *Scand. J. Metall.* **1994**, *23*, 201–208.
28. Xia, C.-H.; Wang, Y.; Wang, J.-J.; Lu, X.-G.; Zhang, L. Thermodynamic assessment of the Co–Fe–Ni system and diffusion study of its fcc phase. *J. Alloys Compd.* **2021**, *853*, 157165. [[CrossRef](#)]
29. Zhang, W.; Du, Y.; Zhang, L.; Xu, H.; Liu, S.; Chen, L. Atomic mobility, diffusivity and diffusion growth simulation for fcc Cu–Mn–Ni alloys. *Calphad* **2011**, *35*, 367–375. [[CrossRef](#)]
30. Hillert, M. The compound energy formalism. *J. Alloys Compd.* **2001**, *320*, 161–176. [[CrossRef](#)]

31. Dinsdale, A.T. SGTE data for pure elements. *Calphad* **1991**, *15*, 317–425. [[CrossRef](#)]
32. Andersson, J.; Ågren, J. Models for numerical treatment of multicomponent diffusion in simple phases. *J. Appl. Phys.* **1992**, *72*, 1350–1355. [[CrossRef](#)]
33. Jönsson, B. On ferromagnetic ordering and lattice diffusion—A simple model. *Z. Met.* **1992**, *83*, 349–355.
34. Redlich, O.; Kister, A.T. Algebraic Representation of Thermodynamic Properties and the Classification of Solutions. *Ind. Eng. Chem.* **1948**, *40*, 345–348. [[CrossRef](#)]
35. Kundrat, D.M. Phase relationships in the Fe-Cr-Mn-Ni-C system at solidification temperatures. *Metall. Mater. Trans. A* **1986**, *17*, 1825–1835. [[CrossRef](#)]
36. Parravano, N. Ternary alloys of iron-nickel-manganese, nickel-manganese-copper, and iron-manganese-copper. *Z. Met.* **1913**, *4*, 171–201.
37. Whittle, D.; Green, A. The measurement of diffusion coefficients in ternary systems. *Scr. Metall.* **1974**, *8*, 883–884. [[CrossRef](#)]
38. Neumann, G.; Tölle, V. Monovacancy and divacancy contributions to self-diffusion in face-centred cubic metals reanalysis for copper, silver, gold, nickel and platinum. *Philos. Mag. A* **1986**, *54*, 619–629. [[CrossRef](#)]

Disclaimer/Publisher’s Note: The statements, opinions and data contained in all publications are solely those of the individual author(s) and contributor(s) and not of MDPI and/or the editor(s). MDPI and/or the editor(s) disclaim responsibility for any injury to people or property resulting from any ideas, methods, instructions or products referred to in the content.